基于多层 ANN 的机器人等离子熔射智能化模型

夏 卫生[1,2]， 张海鸥[2]， 王桂兰[1]， 杨云珍[1]
（1. 华中科技大学 材料成形与模具技术国家重点实验室，武汉 430074；
2. 数字制造装备与技术国家重点实验室，武汉 430074）

夏 卫生

摘 要：分析了机器人等离子熔射过程的神经网络模型的实现方法，基于多层人工神经网络（artificial neural network，ANN）建立了等离子熔射过程的智能化模型. 基于该模型，系统研究了等离子弧电流、熔射距离、机器人扫描间距和速度对主要涂层性能参数—残余应力和孔隙率的影响规律，并通过试验数据库的学习对涂层性能参数进行预测. 结果表明，模型预测结果与试验结果有着很好的吻合，解决了工艺试验结果中仅有离散数据且难以全面反映等离子熔射工艺参数—涂层性能之间复杂非线性关系的难题.

关键词：机器人等离子熔射；人工神经网络；智能化模型；残余应力；孔隙率
中图分类号：TG174.442 文献标识码：A 文章编号：0253－360X(2009)07－0041－04

0 序 言

等离子熔射中如何清晰了解工艺参数之间相互关联以及它们对涂层性能的独立影响规律是成形过程质量控制的难题之一[1,2]. 人工神经网络（artificial meural network，ANN）以其特有的非线性适应性信息处理能力，在神经专家系统、智能控制等领域得到了成功应用[3]，并已发展成为解决材料科学问题的一种有效且强健的建模手段[4－6]. 采用 ANN 方法建立等离子熔射智能化模型，已成为熔射成形质量控制的重要研究方向之一[7,8].

因此，作者采用误差反传神经网络（back propagation，BP）建立等离子熔射智能化模型. 通过对工艺试验数据库的学习与网络训练，形成熔射工艺参数与涂层质量之间关系的神经网络模型. 据此预测涂层性能参数，并进行理论分析.

1 等离子熔射过程的 ANN 模型建立

在 ANN 模型中将等离子熔射工艺参数作为输入矢量，涂层性能参数作为输出矢量. 采用合理的神经元数目来表征工艺参数. 多数参数可用一个神经元表示，但需用 n 个来表征 2^n 种粉末材料类型.

作者采用包含一个隐含层的 BP 网络对等离子熔射过程进行建模，所建立的多层神经网络结构如图 1 所示，隐含层单元数根据网络训练结果确定.

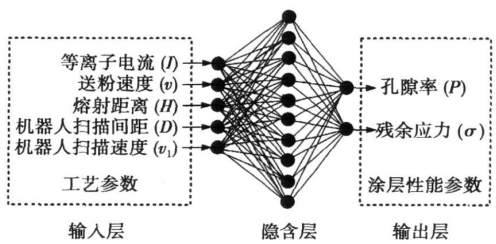

图 1 多层神经网络结构

Fig. 1 Network structure of multi-layer ANN

为提高网络的收敛速度，采用 Levenberg-Marquardt 算法在 Matlab 软件环境中处理所建立的智能化模型. 选取各单元传递函数分别为 tansig 和 purelin 函数，设置 BP 网络的反传函数为 trainlm. 设定训练步数为 1×10^4 步，训练误差小于 1×10^{-20}.

采用正则化方法修正神经网络的训练性能函数来提高 BP 神经网络的泛化能力[9]. 采用网络误差的均方根之和作为神经网络的性能函数 F_{mse} 为

$$F_{mse}=\frac{1}{N}\sum_{i=1}^{N}(e_i)^2=\frac{1}{N}\sum_{i=1}^{N}(t_i-a_i)^2 \qquad (1)$$

收稿日期：2008－07－21
基金项目：国家“863”高技术研究发展计划资助项目（2007AA04Z142）；国家自然科学基金（50675081）；中国博士后科学基金（20080440940）

式中：e_i，t_i 和 a_i 分别为第 i 个训练样本的训练误差、目标输出和网络输出. 而在正则化方法中，调整之后的网络性能函数 F_{reg} 为

$$F_{reg}=\gamma F_{mse}+(1-\gamma)\triangle msw \quad (2)$$

式中：γ 是比例参数；$\triangle msw$ 为所有网络权值平方和的平均值，$\triangle msw=\frac{1}{N}\sum_{j=1}^{n}w_j^2$. 采用新的性能指标函数 F_{reg}，能够在保证网络训练误差尽可能小的情况下使网络具有较小权值，减小网络规模.

2 试验数据库建立

2.1 试验条件与方法

在基体(45 钢，100 mm× 110 mm×4 mm)上熔射合金粉末 ZX. Ni45A，时间 12 min，控制涂层厚度在 0.3～0.4 mm. 路径为 Z 字形变向 90°. 主要等离子熔射工艺参数如表 1 所示. 送粉速度分别为 0.108，0.163，0.197，0.343 g/s，基准值为 0.108 g/s. 采用 X—350A 型 X 射线应力测定仪确定涂层残余应力，用金相分析法确定涂层孔隙率.

表 1 等离子熔射工艺参数

Table 1 Parameters setting during plasma spraying

参数	电流 I/A	电压 U/V	熔射距离 H/mm	扫描间距 D/mm	扫描速度 υ_1/(mm·s^{-1})
变化范围	320～640	50	170～290	8～20	200～500
步长	80	—	40	4	100
基准值	400	50	250	12	300

2.2 数据库设计

建立数据库需要考虑[10]：(1) 单个工艺参数在有限范围内变化，其它参数为基准值；(2) 增加部分细节内容来解决物理限制，如零电压、零电流不能熔射；(3) 部分试验需考虑中间变量.

数据库划分为三类：(1) 有效类，用来定义 ANN 结构，确定神经元特征和调整每层神经元数目；(2) 训练类，用来调整神经网络权值；(3) 测试类，验证训练方案有效性.

3 ANN 预测结果分析与比较

3.1 网络预测能力测定

采用训练后的神经网络对随机选择的一组试验数据进行预测，表 2 为试验结果与 ANN 模型预测结果比较. 由表可知，设置隐含层的神经元数目为 10 时，模型的预测结果最准确，其中孔隙率和残余应力误差分别为 1.59%和 4.88%，可见训练后的网络能够正确地对新知识进行预测. 同时网络的输出与目标输出完全重合，表明网络有很好的记忆能力.

表 2 ANN 模型预测能力测定

Table 2 Prediction ability evaluation of ANN model

各层神经元数目	残余应力 σ/MPa			孔隙率 P(%)		
I∶H∶O	M_R	E_R	误差	M_R	E_R	误差
5∶5∶2	76.20		5.83%	8.12		8.70
5∶10∶2	70.85	72	1.59%	7.84	7.47	4.88
5∶15∶2	68.74		4.53%	7.04		5.76

其中：I，H 和 O 分别为多层 ANN 网络结构中输入层、隐含层与输出层神经元数目；M_R 为 ANN 模型预测结果；E_R 为试验结果

3.2 工艺参数对涂层性能参数的影响

3.2.1 等离子弧电流

等离子弧电流从 320 A 变化到 640 A 时，涂层残余应力、孔隙率的试验曲线和 ANN 预测曲线分别见图 2 和图 3. 由两图可知，ANN 预测曲线与试验数据变化趋势相吻合. 由于电压恒定为 50 V，电流变化等同于功率变化. 当电流过小时，由于粉末不能得到充分熔化，涂层中未熔粉末增多，孔隙率变大，导致涂层残余应力增大；当电流增加到 550 A 后，孔隙率呈现下降趋势，此时熔射到基体上的粉末粒子能够得到充分加热和加速，高速高温的粒子紧紧地结合在一起，降低了涂层孔隙率. 同时由于部分粉末被汽化，残余应力也有所降低. 从图 2 与图 3 也可看出，由于该金属粉末的熔点较低，当电流为 460 A 时，金属涂层具有最小的孔隙率和残余应力，从而具有最好的成形性.

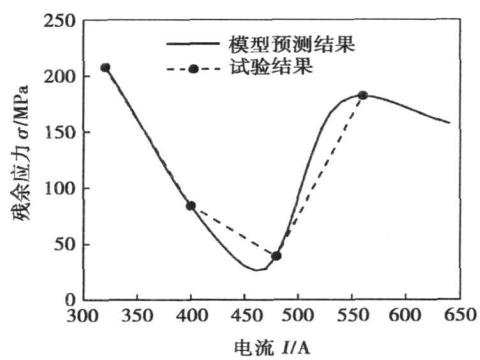

图 2 等离子弧电流对残余应力的影响

Fig 2 Influence of plasma arc current on residual stress

3.2.2 机器人扫描速度

机器人扫描速度从 200 mm/s 变化到 500 mm/s 时，涂层残余应力、孔隙率的试验曲线和ANN预测

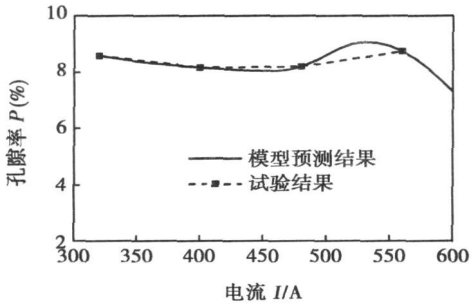

图 3　等离子弧电流对涂层孔隙率的影响

Fig. 3　Influence of plasma arc current on coating porosity

曲线分别见图 4 和图 5. 结果表明，在扫描速度为 200 mm/s 时，涂层具有最小残余应力和较小孔隙率，成形质量较高. 相关研究结果表明，粉末粒子对基体或已熔射涂层的局部加热效应明显强于等离子射流对其的作用[10]. 因此，在其它工艺条件相同的情况下，机器人扫描速度变化将改变熔射范围内瞬时热功率分布，从而影响涂层表面的温度分布. 速度太低将造成涂层局部过热，残余应力增大；而速度过

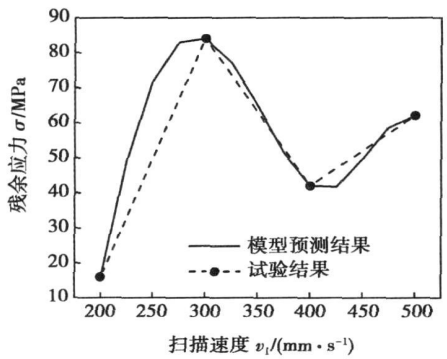

图 4　扫描速度对残余应力的影响

Fig. 4　Influence of scanning speed on residual stress

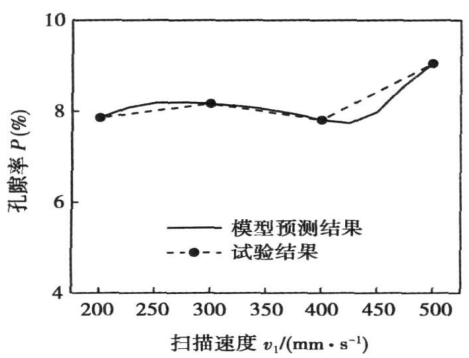

图 5　扫描速度对涂层孔隙率的影响

Fig. 5　Influence of scanning speed on coating porosity

快则降低涂层表面温度，影响金属粉末与涂层结合，最终影响涂层内部的残余应力以及孔隙率.

3.2.3　机器人扫描间距

机器人扫描间距从 8 mm 变化到 20 mm 时，涂层残余应力、孔隙率的试验曲线和 ANN 预测曲线分别见图 6 和图 7. 从两图可以看出，在扫描间距为 17 mm 时，金属涂层具有较小的残余应力，而扫描间距为 20 mm 时金属涂层具有最小的孔隙率. 这主要是因为在其它工艺条件相同的情况下，改变熔射路径的扫描间距会改变相邻熔射道次间涂层的叠加程度，从而改变涂层厚度分布和温度分布，最终影响涂层的残余应力和孔隙率.

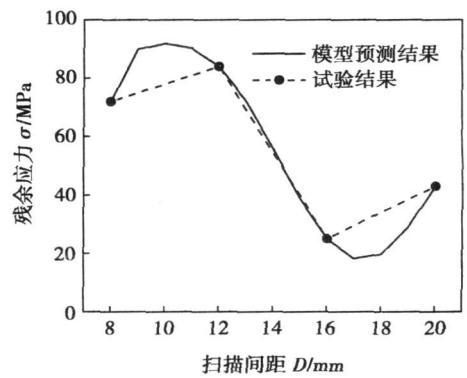

图 6　扫描间距对残余应力的影响

Fig. 6　Influence of scanning space on residual stress

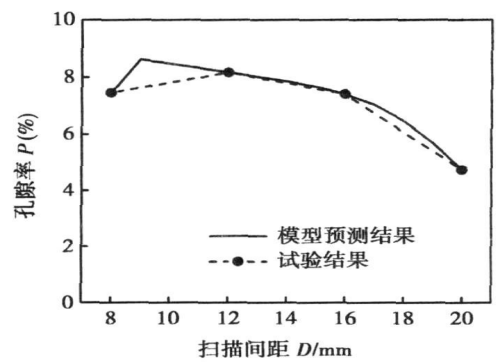

图 7　扫描间距对涂层孔隙率的影响

Fig. 7　Influence of scanning space on coating porosity

3.2.4　熔射距离

熔射距离从 170 mm 变化到 290 mm 时，涂层残余应力、孔隙率的试验曲线和 ANN 预测曲线分别如图 8 和图 9 所示. 由图可知，在熔射距离为 170 mm 和 290 mm 时，金属涂层具有较小的残余应力；在熔射距离为 170 mm，涂层具有最小的孔隙率. 这主要是因为在其它工艺条件相同的情况下，改变喷枪到

基体表面的熔射距离会改变粉末粒子的加热历程，当选用过近的距离时，等离子射流的加热效应会导致涂层表面的温度急剧升高，引起涂层热变形. 同时，粉末粒子在熔射距离过近时，容易被基体表面弹回而影响沉积效率；当喷嘴端面与基体表面距离过远时，粒子减速并冷却，影响粒子与涂层的结合，最终影响涂层的残余应力和成形质量.

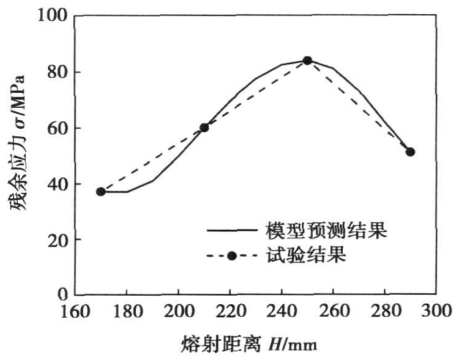

图 8 熔射距离对残余应力的影响

Fig. 8 Influence of spraying distance on residual stress

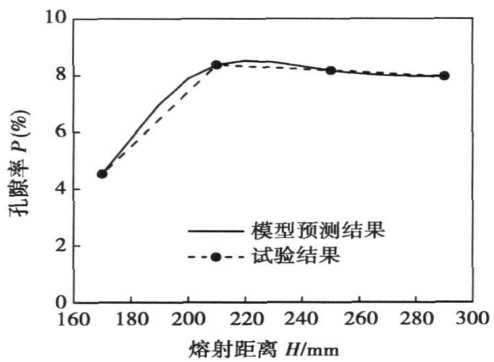

图 9 熔射距离对涂层孔隙率的影响

Fig. 9 Influence of spraying distance on coating porosity

4 结 论

(1) 建立了机器人等离子熔射智能化模型. 通过对工艺试验结果的学习，该模型能够对熔射涂层质量进行全面预测，并能很好地记忆已学习知识，预测值与试验值的变化趋势基本一致.

(2) 根据 ANN 模型预测结果可确定一组合理的熔射工艺参数：等离子弧电流 460 A，熔射距离 170 mm，机器人扫描间距 20 mm，扫描速度 200 mm/s.

(3) 该模型能够应用于机器人等离子熔射智能控制，提供全面描述工艺参数—成形质量之间关系的智能控制规则集.

参考文献：

[1] Guessasma S, Montavon G, Coddet C. Modeling of the APS plasma spray process using artificial neural networks: Basis, requirements and an example[J]. Computational Materials Science, 2004, 29(3): 315—333.

[2] Tucker Jr R C. Integrated thermal spray systems-some practical considerations[C] // Thermal Spray 2001: New Surfaces for a New Millennium. Singapore: ASM International, 2001: 1261—1266.

[3] 李国勇. 智能控制及其 MATLAB 实现[M]. 北京：电子工业出版社，2005.

[4] Bhadeshia H K D H. Neural networks in materials science[J]. ISIJ International, 1999, 39(10): 966—979.

[5] Dussoubs B, Mariaux G, Vardelle A, *et al*. D.C. plasma spraying: effect of arc root fluctuations on particle behavior in the plasma jet [J]. High Temperature Material Processes, 1999, 3(2—3): 235—254.

[6] Gowri S, Shankar G U, Narayanasamy K, *et al*. Expert system for process optimization of atmospheric plasma spraying of high performance ceramics[J]. Journal of Materials Processing Technology, 1997, 63(1—3): 724—732.

[7] Lugscheider E S, Seemann K. Prediction of plasma sprayed coating properties by the use of neural networks[C] // Thermal Spray 2004: Advances in Technology and Application, Osaka, Japan: ASM International, 2004: 459—463.

[8] Guessasma S, Montavon G, Gougeon P, *et al*. Designing expert system using neural computation in view of the control of plasma spray processes[J]. Materials and Design, 2003, 24(7): 497—502.

[9] 许 东，吴 铮. 基于 MATLAB6.x 的系统分析与设计—神经网络[M]. 西安：西安电子科技大学出版社，2002.

[10] Bolot R, Li L, Bonnet R, *et al*. Modeling of the substrate temperature evolution during the APS thermal spray process[C] // Thermal Spray 2003: Advancing the Science and Applying the Technology, Orlando, FL: ASM International, 2003: 949—954.

作者简介：夏卫生，男，1979 年出生，工学博士. 主要从事机器人等离子熔射数字化成形与智能控制、功能涂层与固体氧化物燃料电池制备研究. 发表论文 20 余篇.

Email：xiatianhust@hotmail.com

(FZ) and the average micro-hardness value is 447HV when heat input E= 135 kJ/m is utilized. With heat input increasing to 150 kJ/m, the number of α' phase decreases in FZ, short acicular $\alpha+\beta$ phase become coarser in heat-affected zone(HAZ) of TC11, coarse β grains become larger in HAZ of Ti-24Al-15Nb-1.5Mo and the average micro-hardness value drops to 402HV. The result is attributed to the changed content of alloy elements and lower cooling velocity caused by increasing heat input. The content of element Ti, Al and Nb is changed abruptly in the boundary of the joint, but these elements evenly distribute in each zone and hardly diffuse.

Key words: electron beam welding; dual alloy; heat input; fine texture; microstructure

Microstructural characterization of TC4/Cu/ZQSn10-2-3 diffusion bonded joints ZHAO He, CAO Jian, FENG Jicai (State Key Laboratory of Advanced Welding Production Technology, Harbin Institute of Technology, Harbin 150001, China). p 37—40

Abstract: The experimental investigation on the diffusion bonding of TC4 to ZQSn10-2-3 was carried out in vacuum. $CuSn_3Ti_5$, Cu_3Ti and rich-Pb layer were formed at the interface zone. The maximum joint strength was 102 MPa. Brittle fracture was explored after shear test, and occurred proximity to ZQSn10-2-3 side. Using copper as the interlayer, element Sn and Pb can be avoid diffusing from ZQSn10-2-3 to TC4. Then there were little $CuSn_3Ti_5$ in the interface. Fracture had certain plasticity, and the maximum strength of joint was 196 MPa. The optimum bonding parameters were: bonding temperature T= 830 ℃, bonding pressure p= 10 MPa and bonding time t= 30 min.

Key words: titanium alloy; tin-bronze; diffusion bonding; copper interlayer

Intelligent process modeling of robotic plasma spraying based on multi-layer artificial neural network XIA Weisheng[1,2], ZHANG Haiou[2], WANG Guilan[1], YANG Yunzhen[1] (1. State Key Laboratory of Material Processing and Die & Mould Technology, Huazhong Universiry of Technology, Wuhan 430074, China; 2. State Key Laboratory of Digital Manufacturing Equipment and Technology, Huazhong University of Science & Technology, Wuhan 430074, China). p 41—44

Abstract: The implementation of multi-layer artificial neural networks (ANNs) in robotic plasma spraying was discussed and an intelligent process model was constructed to fully describe the relationships between process parameters and coating properties. Influences of plasma arc current, spray distance, robot scanning space and scanning velocity on coating properties, i. e. residual stress and porosity, were systematically studied based on the present model. Prediction can be effectively carried out after the learning of the experimental database. Theoretical analysis shows the prediction results agree well with the experiments. It is favorable to fully investigate the complex and nonlinear relationships between processing parameters and coating properties as well as to overcome the limited information indicated by the discrete variable in the processing results.

Key words: robotic plasma spraying; artificial neural network; intelligent model; residual stress; porosity

Kinematics and track amendments of intersecting pipe welding robot DU Hongwang[1,2], WANG Zongyi[2], LIU Shaogang[1], ZHAO Yanan[1] (1. College of Mechanical & Electrical Engineering, Harbin Engineering University, Harbin 150001, China; 2. College of Automation, Harbin Engineering University, Harbin 150001, China). p 45—48

Abstract: According to the welding particularity on the junctions of intersecting pipe, the 4 degrees of freedom suspended welding robot was developed and mechanical structure of the body was introduced. Based on the relation of the joints, the kinematics modeling was established with the method of D-H (Denavit-Hartenberg). To overcome the size error and processing error and welding distortion, the welding track was taught in order to ensure welding quality, and then theory track was amended by the linear interpolation. According to the kinematics modeling, the simulation was carried out with SemMechanic. The results of experiments show that the welding quality meet the requirements actually.

Key words: welding robot; kinematics; teaching; linear interpolation

Dynamical simulation on the pressure response of load system of linear friction welding machine YIN Dongdong, DU Suigeng, YU Longqi, MA Yunfeng (Key Laboratory of Ministry of Education for Contemporary Design and Integrated Manufacturing Technology, Northwestern Polytechnical University, Xi'an 710072, China). p 49—52, 56

Abstract: In order to study the closed-loop control qualities of the electro-hydraulic servo load system of the linear friction welding machine on the slipway pressure, closed-loop transfer function of the pressure for the electro-hydraulic servo load system was established according to the relationship between input and output variables, a simulation model was established according to the transfer function and the simulation was carried out. In order to validate reliability of the simulation result, a frequency characteristics experiment of pressure was implemented under closed-loop control, and the system pressure's affect on the pressure's closed-loop response characteristics was specially analyzed. The results show as follows: the emulational and experimental results are anastomosing; the electro-hydraulic servo load system is a second-order inertial & first-order differential link for closed-loop pressure control, the system frequency width is large, and the system stability is high; pressure's closed-loop dynamic response characteristics can be improved by promoting the system pressure.

Key words: linear friction welding machine; electro-hydraulic servo system; dynamic quality; simulation

Study on rapid solidification welding techniques of quenched Cu-Sn alloy foils ZHAI Qiuya, YANG Jinshan, XU Jinfeng, GUO